



HAL
open science

Numerical simulations of outdoor wind effects on smoke spreading along a corridor: Physical and sensitivity analysis

A.J. Wang, B. Manescau, Quentin Serra, K. Chetehouna, Éric Florentin, C. de Izarra

► To cite this version:

A.J. Wang, B. Manescau, Quentin Serra, K. Chetehouna, Éric Florentin, et al.. Numerical simulations of outdoor wind effects on smoke spreading along a corridor: Physical and sensitivity analysis. *International Journal of Thermal Sciences*, 2019, 142, pp.332-347. 10.1016/j.ijthermalsci.2019.02.027 . hal-02134030

HAL Id: hal-02134030

<https://hal.science/hal-02134030>

Submitted on 22 Oct 2021

HAL is a multi-disciplinary open access archive for the deposit and dissemination of scientific research documents, whether they are published or not. The documents may come from teaching and research institutions in France or abroad, or from public or private research centers.

L'archive ouverte pluridisciplinaire **HAL**, est destinée au dépôt et à la diffusion de documents scientifiques de niveau recherche, publiés ou non, émanant des établissements d'enseignement et de recherche français ou étrangers, des laboratoires publics ou privés.



Distributed under a Creative Commons Attribution - NonCommercial 4.0 International License

The Title: Numerical simulations of outdoor wind effects on smoke spreading along a corridor: physical and sensitivity analysis

The Authors: A.J. Wang^{a,*}, B. Manescau^a, Q. Serra^b, K. Chetehouna^a, E. Florentin^b, C. De Izarra^a

Affiliation : ^a INSA Centre Val de Loire, Univ. Orléans, PRISME, EA 4229, F-18022 Bourges, France

^b INSA Centre Val de Loire, Univ. Orléans, Univ. Tours, LaMé, EA 7494, F-18022 Bourges,
France

Corresponding Author: Aijuan Wang

Address: 88 Boulevard Lahitolle, 18000 Bourges, France

E-mail: aijuan.wang@insa-cvl.fr

Tel: +33 06 68 47 13 18

Numerical simulations of outdoor wind effects on smoke spreading along a corridor: physical and sensitivity analysis

A.J. Wang^{a,*}, B. Manescau^a, Q. Serra^b, K. Chetehouna^a, E. Florentin^b, C. De Izarra^a

^a INSA Centre Val de Loire, Univ. Orléans, PRISME, EA 4229, F-18022 Bourges, France

^b INSA Centre Val de Loire, Univ. Orléans, Univ. Tours, LaMé, EA 7494, F-18022 Bourges, France

Abstract

In this study, the effects of outdoor wind on smoke movements along a corridor were investigated using a CFD code: Fire Dynamics Simulator (FDS). Firstly, a comparison between experimental and numerical results was carried out by varying outdoor wind velocity from 0 to 12.12 m/s, and good agreement was found between the two. Secondly, from the numerical data, it was found that smoke stratification state in the corridor depends on Froude number (Fr) and it can be divided into three cases: stable buoyant stratification ($Fr < 0.38$), unstable buoyant stratification ($0.38 \leq Fr < 0.76$) and failed stratification ($Fr \geq 0.76$). When $Fr \geq 0.76$, smoke stratification is completely disturbed and smoke occupies the entire volume of the compartment, highlighting a risk of toxicity to people. In addition, it was observed that the velocity of the outdoor wind could influence the concentration of O₂, CO₂, CO and visibility in the corridor and smoke exhaust. In view of the large amount of input data used for the numerical simulation, a global sensitivity analysis was conducted on parameters related to the material, fuel and combustion model. The analysis demonstrated that the main parameters affecting the smoke temperature near the ceiling are the mass flux of fuel and the activation energy. An analytical model was proposed to predict the time evolution of the quantity of interest for arbitrary values of mass flux and activation energy.

Keywords: Smoke spread, FDS, Corridor, Outdoor wind, Sensitivity analysis

1. Introduction

The increase in the world population and economic growth in recent decades have favored the construction of buildings. These developments present many challenges to fire safety engineering, however, because the

* Corresponding author. Tel: +33 0668471318.
E-mail address: aijuan.wang@insa-cvl.fr.

number of victims is usually very high during building fires. The fire that took place at the Paris-Opéra hotel in France in April 2005, for instance, the worst fire in France in the last 60 years, left 24 people dead, 11 of them children, and dozens injured. In order to reduce the number of deaths, fire safety engineering has focused on understanding the different phenomena present in a building fire [1]. Among these phenomena, Paul et al. [2] and Hull et al. [3] showed that smoke is the main cause of death due to toxicity. The smoke plume can be hazardous for people in two different ways: the toxic gases in smoke, such as carbon dioxide, are a fatal hazard [2][3], and the smoke can make it difficult to rescue and evacuate people as it reduces visibility. In a compartment fire, it is therefore very important to know the characteristics of the smoke spreads. The parameters that have an effect on the smoke spread are mechanical ventilation and external atmospheric conditions. Generally, mechanical ventilation ensures smoke exhaust; however, external atmospheric conditions can disturb smoke flow. Smoke flows depend essentially on physical properties such as expansion, thermal pressure, thermal buoyancy, and wind effect. Variation in one of these parameters, such as the external wind, can affect fire dynamics [4][5][6] and smoke behavior [7][8] inside a compartment. In the context of fire safety, it is important to study the effects of external atmospheric conditions on smoke spread in a compartment.

During a fire in a room, the presence of external wind through an opening contributes to disturbance of the smoke flow, which can impair the extraction process, thereby increasing the risk of death. Several studies have been carried out in recent years to provide knowledge for fire safety engineering, including many full-scale [9][10] and reduced-scale [11][12][13][14] experimental investigations.

At full scale, Tian et al. [9] showed that the more the wind velocity increases, the more smoke temperature near the floor increases, in order to converge to the smoke temperature near the ceiling. Considering this, they highlighted that above a certain critical value of outdoor wind velocity, smoke stratification was disturbed and smoke occupied the entire volume of the compartment. Zhong et al. [10] studied the development of smoke as a function of heat release rate and wind. They found that at the beginning of the fire, wind speed was higher than smoke speed and wind speed became negligible when the fire reached its maximum. From scaling laws in Ref. [15][16], small-scale experimental tests have been developed. Li et al. [11] studied the influence of external wind velocity on the smoke flow in a small-scale facility. They showed that the driving forces of smoke flows through a high-rise building were modified according to the intensity of the external wind. Fan et al. [14] then obtained a correlation giving the transverse distribution of the temperature field of the smoke below the ceiling as a function of the distance from the fire.

In addition to the experimental studies cited above, numerical simulations on smoke propagation in a compartment have also been conducted. Li et al. [17] simulated smoke flows in a reduced scale (1:12) corridor under natural ventilation conditions using CFD FDS. They compared numerical data with experimental data and emphasized that FDS was able to simulate the temperature field and the level of smoke stratification for different heat release rates (HRR). Similarly, Zhao et al. [18] achieved a good agreement between numerical results and experimental data by studying the impact of openings on the smoke flow during a fire in a confined enclosure. Yang et al. [19] simulated smoke flow along a tunnel in fire as a function of the extraction rate using the CFD software PHOENICS. They observed a similarity between analytical and numerical results. Similar to the results of Vauquelin [20], they showed that backflow of the smoke in the downstream part could occur when the extraction speed was too low. Weng et al. [21] performed numerical simulations on the smoke flow in a subway tunnel fire equipped with an extraction system. Their results revealed that the temperature and level of smoke stratification under the tunnel ceiling in the longitudinal direction increased with the HRR.

These different experiments and numerical studies have provided information on the behavior of smoke in a compartment fire. However, in order to obtain accurate output results, it is necessary to define the input data correctly by carrying out a sensitivity analysis in order to find out the input parameters that have the most influence on the output data. Two kinds of approach are classically used to achieve this: local and global approaches. For example, Batiot et al. [22] applied local and global sensitivity analysis on Arrhenius parameters in order to describe the kinetics of solid thermal degradation during fire phenomena, by determining four parameters (A, E, n and v). They stressed the specific role of A and E on the equation and showed the role and the influence of these parameters in the differential equation used to model the mass loss rate of a solid fuel as a function of the temperature and time. Xiao et al. [23] applied global sensitivity analysis to an environmental model, LevelE. The sensitivity indices used the energy distribution of the model output over different frequency bands as the quantitative feature of the model output. Lamboni et al. [24] performed global sensitivity analysis for dynamic crop models to help researchers make better decisions about the growing season of crops. Just like the application of sensitivity analysis in the field above, it can be a useful methodology in determining smoke behavior in fires.

Because of the computational burden associated with classical global analysis, estimates of the sensitivity indices are computed by using a Polynomial Chaos expansion of the quantity of interest [25].

Most of the numerical simulations that focused on the propagation of smoke in a ventilated or unventilated enclosure studied the level of smoke stratification as a function of the temperature profile and velocity. However, these numerical studies do not take into account the effect of the external wind on smoke stratification in a corridor

adjacent to a burning room with an opening. Using the data obtained by Li et al. [11], the aim of the present study was to highlight the ability of the Fire Dynamics Simulator (FDS) to study smoke behavior according to the variation in outdoor wind velocity. This work, through a mesh resolution [26][27], consists in reproducing the experimental conditions obtained in the work of Li et al. [11]. The calculations were carried out using the ARTEMIS cluster of the “Région Centre Val de Loire – France”. The calculation time was 9 hours with a time step of 0.01 s using 20 CPU. Fire modelling was done with a mesh size of 5cm based on the finite rate combustion using Arrhenius parameters. The reactive flows were modelled using the Deardorff turbulence model and the Eddy Dissipation Concept (EDC). The fire source was modelled as a gas burner for which the inlet parameter is the fuel mass flux obtained from experiment.

In this work, a CFD approach was proposed to evaluate the effects of outdoor wind on the smoke spread induced by an adjacent compartment fire. In order to highlight the influence of the input parameters used as initial conditions in the computational modelling, a global sensitivity analysis was performed. This paper is organized as follows: Section 2 presents the physical and numerical modelling, Section 3 gives an overview of the global sensitivity analysis methodology with polynomial chaos expansion, Section 4 focuses on numerical results and global sensitivity analysis, and Section 5 presents the conclusions.

2. Physical and numerical modelling

2.1. Governing equations

The simulations were carried out using the CFD code Fire Dynamics Simulator (FDS) version 6.6.0 [26]. It solves the Navier-Stokes equations using an explicit finite difference scheme. As a CFD code, FDS models the thermally driven flow with an emphasis on smoke and heat transport. It is a large eddy simulation (LES) model using a uniform mesh, and has parallel computing capability using Message-Passing Interface (MPI) [28]. Reactive flows are modelled using a turbulence model based on a LES approach, a combustion model based on the Eddy Dissipation Concept (EDC) and a thermal radiation model based on a gray gas model for the radiation absorption coefficient [27][29].

The models are based on the numerical solving of Navier-Stokes equations. These equations calculate mass, momentum, species and energy conservation [27]:

$$\frac{\partial \rho}{\partial t} + \frac{\partial}{\partial x_j} (\rho u_j) = 0 \quad (1)$$

$$\frac{\partial}{\partial t}(\rho u_j) + \frac{\partial}{\partial x_j}(\rho u_i u_j) = -\frac{\partial p}{\partial x_i} + \rho g_i + \frac{\partial}{\partial x_j} \left\{ \mu \left(\frac{\partial u_i}{\partial x_j} + \frac{\partial u_j}{\partial x_i} - \frac{2}{3} \delta_{ij} \frac{\partial u_i}{\partial x_i} \right) \right\} \quad (2)$$

$$\frac{\partial \rho Y_{k^*}}{\partial t} + \frac{\partial}{\partial x_j} \rho u_j Y_{k^*} = \frac{\partial}{\partial x_j} \left\{ (\rho D)_{k^*} \frac{\partial Y_{k^*}}{\partial x_j} \right\} + \dot{\omega}_{k^*} \quad (3)$$

$$\frac{\partial}{\partial t}(\rho h) + \frac{\partial}{\partial x_j}(\rho u_i h) = \frac{dp}{dt} + \dot{q}''' + \lambda \frac{\partial^2 T}{\partial x_j^2} + \sum \frac{\partial}{\partial x_j} \left\{ h_{k^*} (\rho D)_{k^*} \frac{\partial Y_{k^*}}{\partial x_j} \right\} - \frac{\partial}{\partial x_j} \dot{q}''_{r,j} \quad (4)$$

Eq.(1) is the mass conservation equation, Eq.(2) is the momentum conservation equation, Eq.(3) is the species conservation equation, and Eq.(4) is the energy conservation equation.

2.2. Fire modelling

In this work, modelling was carried out using the Deardorff turbulence model and extinction model based on a critical flame temperature. The combustion model is based on the finite rate combustion using Arrhenius parameters (A: pre-exponential factor and E_a : activation energy). The fire source was modelled as a gas burner using butane as fuel with mass flux given by the experimental data [11]. The combustion heat of butane is 45182.83 kJ/kg.

2.3. Computational domain and boundary conditions

The experimental setup used as reference in the current numerical study represents a reduced scale (1:3) of a facility which contains a corridor and a fire room [11]. As shown in Fig. 1, the dimensions of the corridor were 5.5 m (length) \times 0.7 m (width) \times 0.9 m (height) and the dimensions of the fire room were 2.0 m (length) \times 1.7 m (width) \times 1.0 m (height). The corridor and fire room were connected by a door whose dimensions were 0.7 m long by 0.3 m wide. The window in the fire room was opposite to the door and its dimensions were 0.5 m (width) \times 0.5 m (height). The ceilings and floors of the corridor and fire room were made of steel plate with a thickness of 2.5 mm.

As indicated in Fig. 2, the fire source, a gas burner using liquefied petroleum gas as fuel, was located in the middle of the fire room. The fuel supply rates of the gas burner were controlled and monitored by a flow meter. The HRR in the experiments was determined by multiplying the mass flow rate and the combustion heat of liquefied petroleum gas. The fire size can be scaled up to 96.2 kW of HRR, which corresponds to 1.5 MW full-scale.

The wind can blow into the fire room through the window and the outdoor wind was generated by the fan and a static pressure box. The velocity of the outdoor wind was adjusted by changing the AC frequency of the

frequency converter. The velocity of the outdoor wind varied from 0 to 7.0 m/s and the corresponding full-scale outdoor wind velocity range was 0-12.12 m/s according to the scaling law of Froude modelling [15][16]. Varying the wind velocity, eight experiments were conducted at an HRR of 96.2 kW, equaling 1.5MW full-scale.

The experiments were carried out with ambient temperature ranging from 6 °C to 16 °C. K-type thermocouples with an accuracy of ± 1 °C were used for the temperature measurements in the corridor and fire room. Hot wire wind speed meters were applied to measure the velocity of smoke.

In order to model the geometry and the boundary conditions of the setup used during the experimental tests [11], four computational domains were necessary (Fig. 2). The two domains in the center part represented the fire room and corridor. The other two domains respectively connected to the corridor and the fire room were the openings. These two openings made it possible to simulate wind blowing into room through the window and the smoke spreading out from the corridor. The walls of the corridor and fire room were made of steel having a density of 7850 kg/m³, a thermal conductivity of 46 W/(m·K)⁻¹, a specific heat of 0.5 kJ/(kg·K), and an emissivity of 0.9.

In simulations, the boundary condition at the window was modeled as an opening in the case without wind. With wind, a constant flow rate was set at the window using the velocity boundary condition in FDS. In order to remain consistent with the experimental tests, a waiting time of 150 s was defined before activation of the outdoor wind velocity in the modelling. The simulations were performed in eight cases ($V_w=0, 1, 2, 3, 4, 5, 6, 7$ m/s, which correspond to $V_w=0, 1.73, 3.46, 5.20, 6.93, 8.66, 10.39, 12.12$ m/s full-scale). Similarly, the simulation results were converted into full-scale data according to the Froude number.

The smoke temperature, smoke velocity, concentration of O₂, CO and visibility in the corridor were measured by setting different devices in the plane (Y=0.5 m), near the exit of the corridor (X=5.4 m), at different heights (Z=85, 70, 55, 40, 25 cm). In order to obtain more details about the distribution of temperature, velocity, concentration of O₂ and CO₂, and visibility, slice fields were also set up in the plane Y=0.5 m.

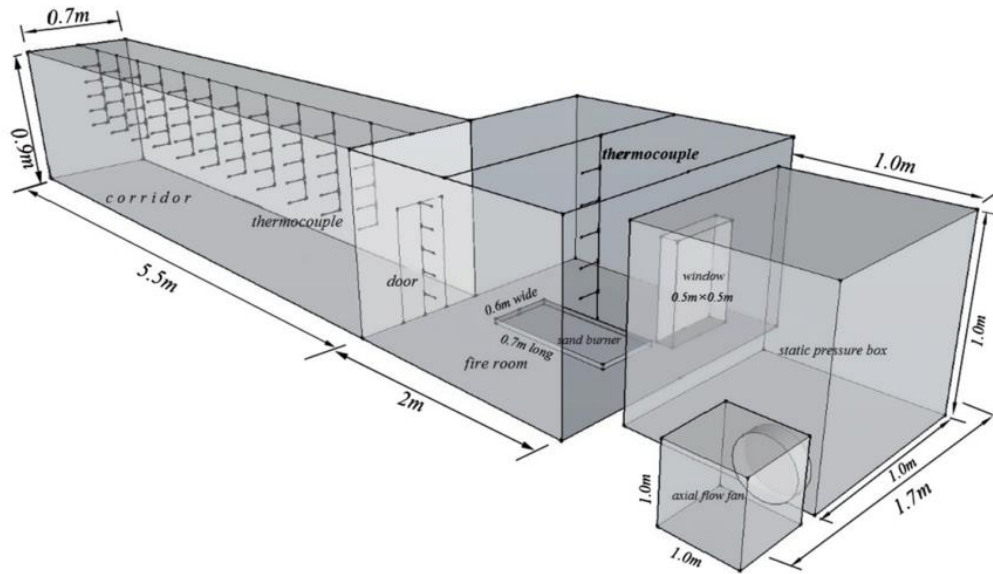


Fig. 1. Schematic view of the experimental corridor and fire room in Ref[11]

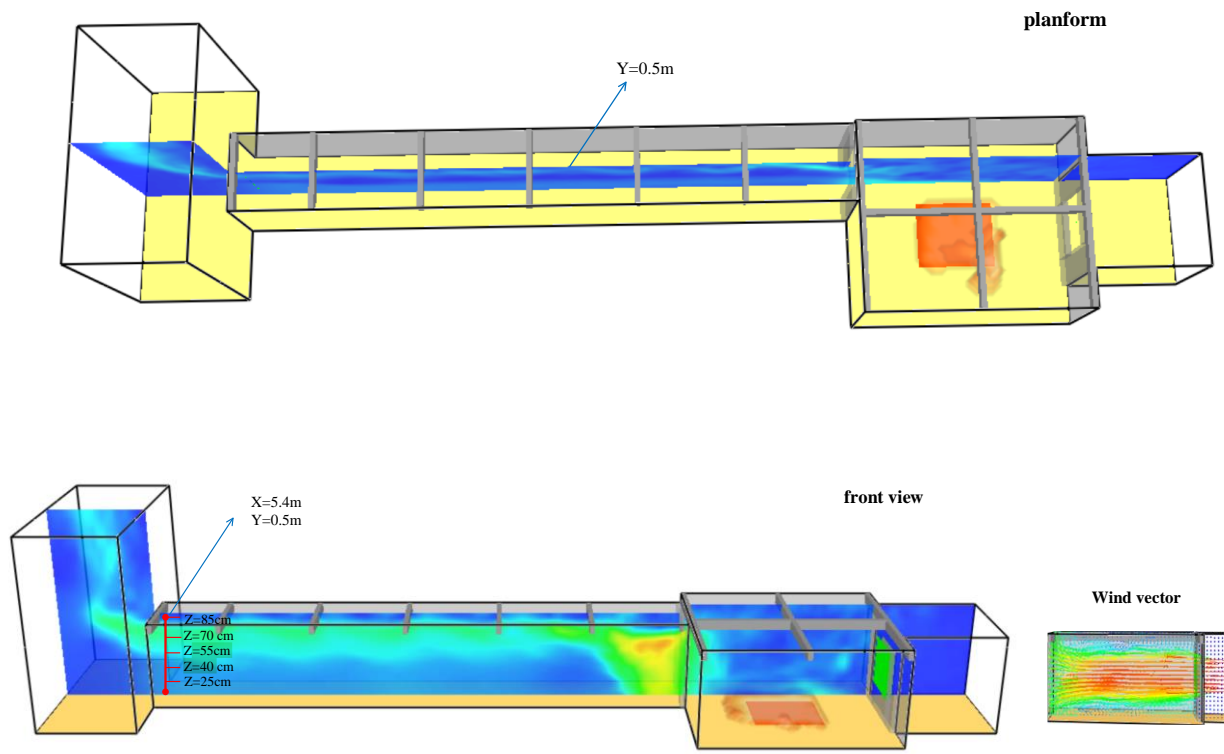


Fig. 2. Geometry of computational domain

2.4. Mesh resolution

For numerical studies, it is important to choose the correct mesh size in order to obtain accurate simulation results. FDS provides a range of mesh sizes for mesh resolution. From a Poisson solver based on the Fast Fourier Transform (FFT), it is possible to obtain good numerical resolution by solving the governing equations. The mesh size was chosen in accordance with the recommendations made in the numerical studies [30][31]. An optimal mesh size should meet two requirements: good results in terms of accuracy and a short calculation time. The optimal mesh size of the domain is given by the non-dimensional expression $D^*/\delta x$, where δx is the nominal mesh size and D^* is the characteristic fire diameter [26]. The characteristic fire diameter D^* is determined using equation (5):

$$D^* = \left(\frac{\dot{Q}}{\rho_{\infty} c_p T_{\infty} \sqrt{g}} \right)^{2/5} \quad (5)$$

where D^* denotes the characteristic fire diameter, \dot{Q} the Heat Release Rate and c_p the specific heat.

Based on several experiments, the U.S. Nuclear Regulatory Commission recommends that the numerical range of $D^*/\delta x$ be between 4 and 16 for simulations to produce favorable results at a moderate computational cost, since the larger the value of $D^*/\delta x$ used in the simulation, the more accurate the simulation result. Hence, the range of mesh sizes can be obtained by the following equation [30][31]:

$$\frac{D^*}{16} \leq \delta x \leq \frac{D^*}{4} \quad (6)$$

After calculation, the range of mesh sizes was found to be: (0.0625 m, 0.25 m). Therefore, four different mesh sizes were used: 20 cm, 10 cm, 5 cm and 2.5 cm. Fig. 3 (a) and Fig. 3 (b) present the comparisons between experiment and FDS predictions for these four different meshes. The comparisons were carried out on the evolution of the smoke temperature and smoke velocity, both measured 70 cm above the ground and in the centerline of the corridor near the exit.

It can be seen that the numerical results obtained with mesh sizes of 5 cm and 2.5 cm converge with the experimental results while the results of the 20 cm and 10 cm meshes diverge. Moreover, the 2.5 cm mesh gives more accurate numerical results than the 5 cm mesh. As shown in table 1, the Relative Gap of the calculation with the 2.5 cm mesh (3.85%) is slightly smaller than the calculation with a 5 cm mesh (6.83%). The Relative Gap(RG) is obtained by [32]:

$$RG = 100 \times \frac{\sqrt{\sum_{i=1}^n (y_{pre,i} - y_{exp,i})^2}}{\sqrt{\sum_{i=1}^n (y_{exp,i})^2}} \quad (7)$$

where y_{pre} is a predicted value, y_{exp} is an experimental value and n is the number of experimental points.

However, the calculation time with the 2.5 cm mesh is 10 times longer than with the 5 cm mesh. In addition, the relative gap of the 5 cm mesh is close to that of the 2.5 cm mesh. As it represents the best trade-off between precision and calculation time, the 5 cm mesh was used for the following calculations.

With the 5 cm mesh, the total number of cells is 94920 and the simulation time is 1000 s with a time step of 0.010 s. The calculations were carried out using 20 processors in the ARTEMIS cluster of the “Région Centre Val de Loire – France” and each computation took about 9.6 h.

Fig. 3 (a) and Fig. 3 (b) show that the numerical results obtained with the 5 cm mesh are in agreement with experimental data as regards the evolution of smoke temperature and smoke velocity [11]. This indicates that with a 5 cm mesh, the boundary conditions can be satisfactorily modeled by FDS and that the interaction between wind and smoke flow can be reproduced.

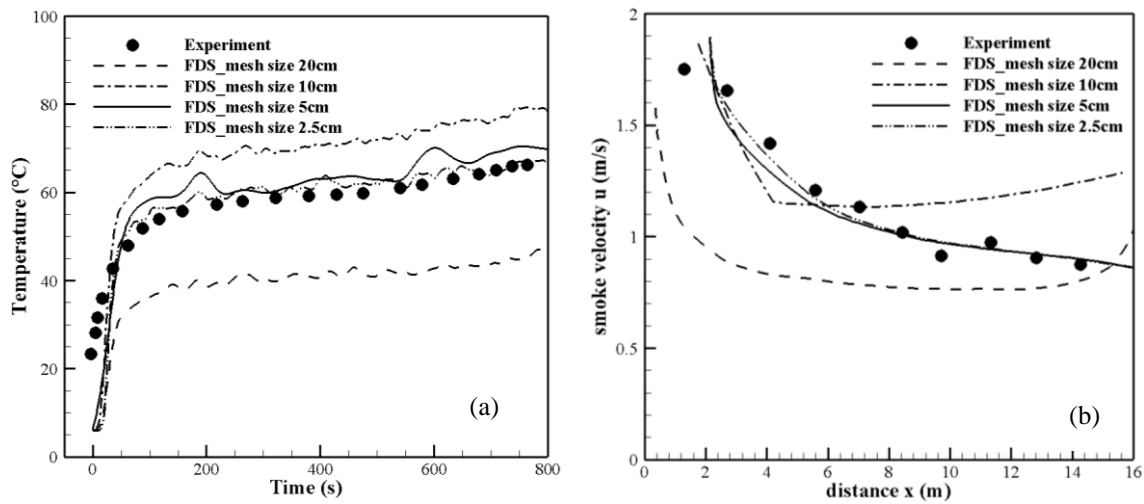


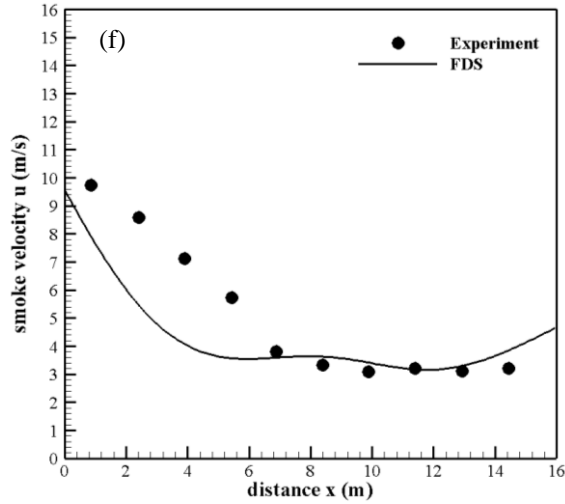
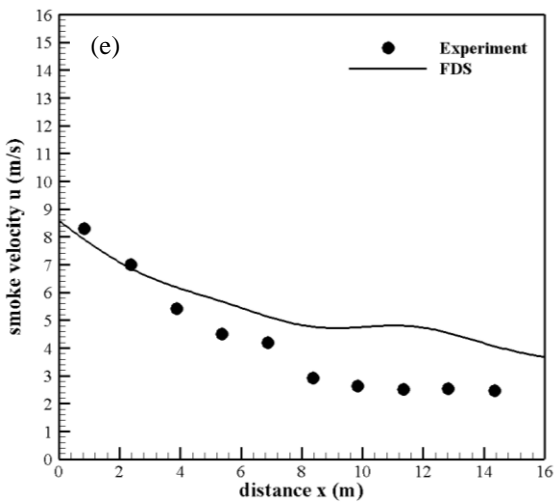
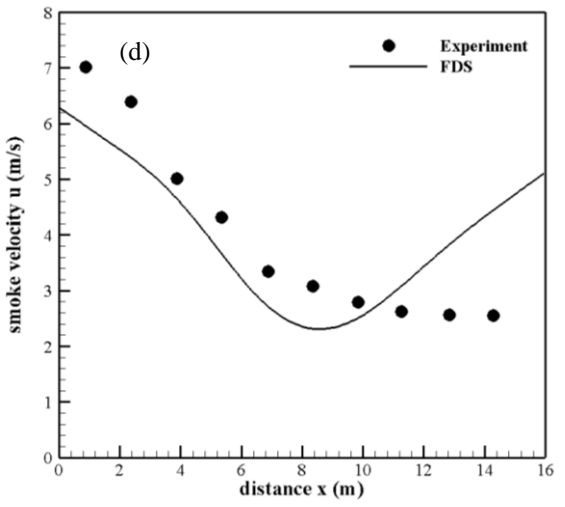
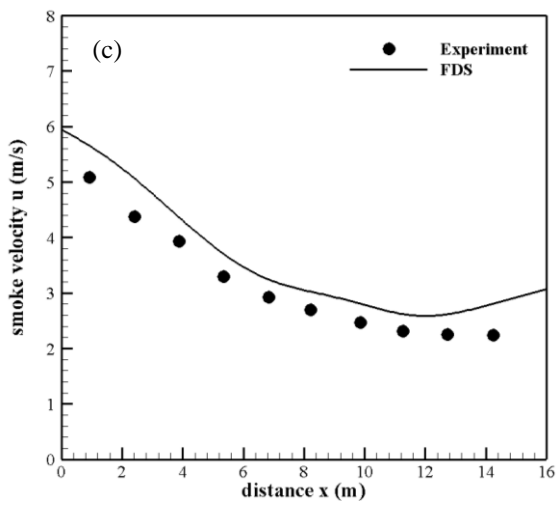
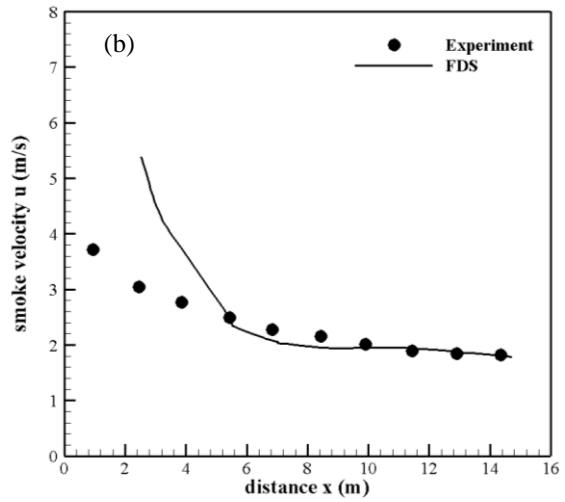
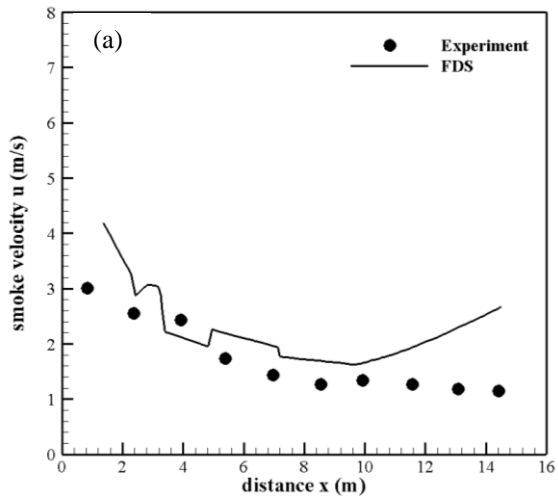
Fig. 3. The influence of grid cells on: (a) temperature at a height of 70 cm; (b) smoke velocity without wind at a height of 70 cm [11]

Table 1 Results of different numerical grid mesh sizes

Numerical grid	Number of cells	Relative Gap (%)		CPU time (h)
		Temperature (°C)	Smoke velocity (m/s)	
Mesh size 20cm	1685	31.06	33.17	1.2
Mesh size 10cm	11865	19.76	16.91	4.4
Mesh size 5cm	94920	6.06	6.23	9.6
Mesh size 2.5cm	759360	3.80	3.85	92.2

Fig. 4 plots the smoke velocity decays with different wind velocities: (a) $V_w=1.73$ m/s; (b) $V_w=3.46$ m/s; (c) $V_w=5.20$ m/s; (d) $V_w=6.93$ m/s; (e) $V_w=8.66$ m/s; (f) $V_w=10.93$ m/s; (g) $V_w=12.12$ m/s at 70 cm height. It can be

seen that the predictions of the evolution of smoke velocities are similar to those of the experimental data [11]. Since the velocities were measured at a height of 70 cm in the experiments, these values are in fact averages. Therefore, it is possible that for some values of the smoke velocity, the experimental data are underestimated or overestimated. In these conditions, predictions are overestimated at the start or at the end of the curves Fig. 4(a-b-d). However, good agreement between prediction and experiment is observed in the other pictures (Fig. 4(c-e-f-g)). It can be concluded from these different comparisons that the choice of a 5 cm mesh is suitable and that it can deal with reactive flows with a good accuracy. Leakage was neglected during the modelling, as the amount of leakage in the experiment is unknown. It is possible, therefore, that some simulation results may be under- or over-estimated. Overall, however, the predictions of the simulations are acceptable.



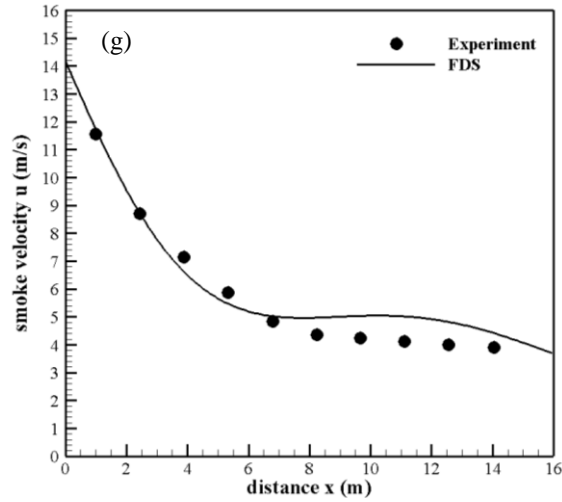


Fig. 4. Smoke velocity with: (a) $V_w=1.73$ m/s; (b) $V_w=3.46$ m/s; (c) $V_w=5.20$ m/s; (d) $V_w=6.93$ m/s; (e) $V_w=8.66$ m/s; (f) $V_w=10.93$ m/s; (g) $V_w=12.12$ m/s at a height of 70 cm of FDS and experimental results [11]

3. Sensitivity analysis methodology

3.1. Global sensitivity analysis

The aim of sensitivity analysis is to quantify the influence of the variation of an input parameter on the variation of an output, also called quantity of interest. In the present study, the quantity of interest is the predicted smoke temperature near the ceiling ($X=5.4$ m, $Y=0.5$ m, $Z=85$ cm), filtered by a Savitzky-Golay algorithm (3rd order) to eliminate high-frequency variations of temperature. It is expressed as a mapping of the input parameters x_i for $i = 1..r$, where r is the number of parameters, and the dependence in time is omitted to simplify the notations, as:

$$T = \mathcal{M}(x_1, \dots, x_r) \quad (8)$$

Generally, there are two kinds of sensitivity analysis: local sensitivity analysis and global sensitivity analysis. The local sensitivity analysis is a simple approach in which the sensitivity indices are directly related to the derivatives of the quantity of interest with respect to each parameter. It is called local because the local indices are only valid in a neighborhood of the nominal value [33]. While local approaches are restricted to the vicinity of the prescribed deterministic values, global sensitivity takes into account the entire domain of variation of each parameter.

To extend the approach in the case of larger variations of parameters, a probabilistic framework is adopted. Lacking knowledge on the probability density functions of the inputs, we assume that each of the parameters follows a uniform law with a $\pm 10\%$ variation around its nominal value.

Of interest in this paper are the Sobol' sensitivity indices. These indices are often associated to an ANOVA (ANalysis Of VAriance) decomposition, which consists in the decomposition of the model response into main effects and interactions [34]:

$$T = \mathcal{M}(x_1, \dots, x_r) = M_0 + \sum_{i=1}^r M_i(x_i) + \sum_{1 \leq i < j \leq r} M_{ij}(x_i, x_j) + \dots + M_{1, \dots, r}(x_1, \dots, x_r) \quad (9)$$

The decomposition is unique if summands satisfy the properties [35]:

$$M_0 = \int \mathcal{M}(x_1, \dots, x_r) dx_1 \dots dx_r \quad (10)$$

$$\int \mathcal{M}(x_{i_1}, \dots, x_{i_s}) dx_{i_1} \dots dx_{i_s} = 0 \text{ for } 1 \leq i_1 < \dots < i_s \leq r \quad (11)$$

The variance of the model response according to variation of inputs can be derived as a sum of partial variances as follows:

$$\text{var}(T) = D = \sum_{i=1}^r D_i + \sum_{1 \leq i < j \leq r} D_{ij} + \dots + D_{1, \dots, r} \quad (12)$$

The partial variances D_{i_1, \dots, i_s} are defined by:

$$D_{i_1, \dots, i_s} = \int M_{i_1, \dots, i_s}(x_{i_1}, \dots, x_{i_s})^2 dx_{i_1} \dots dx_{i_s} \quad (13)$$

Then the Sobol' indices can be derived according to

$$S_{i_1, \dots, i_s} = \frac{D_{i_1, \dots, i_s}}{D} \quad (14)$$

Crude Monte Carlo simulations or sampling based techniques can be applied to obtain these indices, but the associated numerical is prohibitive for computationally demanding models such as those used in this paper. To overcome this difficulty, the exact model provided by simulations was substituted by an analytical approximation, called metamodel, for which the computation of Sobol' indices is exact and analytical. In this paper, a polynomial chaos expansion was used as metamodel to derive the sensitivity indices.

3.2. Polynomial Chaos Expansion

The Polynomial Chaos (PC) expansion consists in the projection of the model M on the space spanned by a family of N_p orthogonal polynomials:

$$\mathcal{M}(x_1, \dots, x_r) \approx \tilde{\mathcal{M}}(x_1, \dots, x_r) = \sum_{\alpha \in A_\alpha} Y_\alpha \Phi_\alpha(x_1, \dots, x_r) \quad (15)$$

where A_α is a finite set of vectors of positive integers $\alpha = (\alpha_{(1)}, \dots, \alpha_{(r)})$ such as $\text{card}(A_\alpha) = N_p$. Each of the multivariate polynomials Φ_α can be expressed as a product of monivariate polynomials $\Psi_{\alpha_{(i)}}$ of order $\alpha_{(i)}$:

$$\Phi_\alpha(x_1, \dots, x_r) = \Psi_{\alpha_{(1)}}(x_1) \times \dots \times \Psi_{\alpha_{(r)}}(x_r)$$

Legendre polynomials were used here because of the assumption of a uniform probability density function for each input parameter. To reduce the number of stochastic coefficients and thus the computational burden, a classical truncation criterion consists in prescribing the constraint: $\sum_{i=1}^r \alpha_{(i)} \leq p$, where p is the maximum order allowed for each monivariate polynomial.

The interest in such a decomposition is that, due to orthonormal properties of the family of polynomials, the mean \tilde{M}_0 , the variance \tilde{D} , the first-order Sobol' indices \tilde{S}_i and the total sensitivity indices $\tilde{S}t_i$ of the metamodel can be computed as analytical functions of the chaos coefficients Y_α [36]:

$$\tilde{M}_0 = \int \tilde{M}(x_1, \dots, x_r) dx_1 \dots dx_r = Y_{\{0, \dots, 0\}} \quad (16)$$

$$\tilde{D} = \int (\tilde{M}(x_1, \dots, x_r) - \tilde{M}_0)^2 dx_1 \dots dx_r = \sum_{\alpha \in A_\alpha \setminus \{0, \dots, 0\}} Y_\alpha^2 \quad (17)$$

$$\tilde{S}_i = \frac{\sum_{\alpha \in A_\alpha^{(i)}} Y_\alpha^2}{\tilde{D}} \text{ with } A_\alpha^{(i)} = \{(\alpha_{(1)}, \dots, \alpha_{(r)}) \text{ such as : } \alpha_{(i)} \neq 0 \text{ and } \alpha_{(j)} = 0 \text{ for } j \neq i\} \quad (18)$$

$$\tilde{S}t_i = \frac{\sum_{\alpha \in At_\alpha^{(i)}} Y_\alpha^2}{\tilde{D}} \text{ with } At_\alpha^{(i)} = \{(\alpha_{(1)}, \dots, \alpha_{(r)}) \text{ such as : } \alpha_{(i)} \neq 0\} \quad (19)$$

To compute the chaos coefficients Y_α , intrusive and non-intrusive approaches can be used. The intrusive approach [37] consists in using PC expansion as an a priori function in the numerical solver. The development of a specific code is needed. It results in a single run of a very large problem. Here we only consider non-intrusive techniques, in which the chaos coefficients are evaluated with repeated runs of a determinist program. Chaos coefficients can be evaluated by projection or by regression [38].

Here, we apply the second technique: it consists in searching the set of coefficients minimizing in the least square sense the L_2 distance between the model and the metamodel. This regression approach leads to:

$$\{Y_\alpha\} = \operatorname{argmin} \left(\frac{1}{Q} \sum_{q=1}^Q \left(\mathcal{M}(x_{1,q}, \dots, x_{r,q}) - \sum_{\alpha \in A_\alpha} Y_\alpha \Phi_\alpha(x_{1,q}, \dots, x_{r,q}) \right)^2 \right) \quad (20)$$

The system is solved in a mean least square sense with a number Q of sampling points $(x_{1,q}, \dots, x_{r,q})$ larger than the number of coefficients to be identified. Typically, in the literature, the number of sampling points is equal to twice the number of polynomial coefficients. In this study, the metamodel is computed using second-order Legendre polynomials. This leads to $N_p = 36$ stochastic modes, so that the number of sampling points is $Q = 72$. Roots of the third-order Legendre polynomial: $\Psi_3(x_{i,q}) = 0$ are chosen as sampling points. The results presented here were validated using the jackknife technique with 100 replications of a random subset of 70 samples.

4. Results and discussion

In this section, the numerical results with different wind velocities ($V_w=1.73$ m/s, 3.46 m/s, 5.20 m/s, 6.93 m/s, 8.66 m/s, 10.93 m/s, 12.12 m/s) are discussed in terms of the effects of outdoor wind on smoke stratification and smoke extraction. A global sensitivity analysis was carried out in order to determine the effects of the input parameters on the output data. The target input parameters are mass flux (MF) of fuel, the material properties (conductivity λ , emissivity ϵ , density ρ and specific heat c_p) and the Arrhenius parameters (A , E_a). The target output data is the smoke temperature near the ceiling.

4.1. Effects of outdoor wind on smoke stratification

In Li et al. [11], it was shown that the more wind velocity increased, the more severely the smoke stratification was disturbed. This observation was obtained by comparing the smoke temperature near the floor (height=25 cm) and the smoke temperature near the ceiling (height=85 cm). The tests were performed for three velocities. The results showed that above a wind velocity of 3.46 m/s, the smoke temperatures near the floor and the ceiling were similar. This similarity was taken to imply that the smoke occupied the entire corridor volume due to the absence of smoke stratification. The FDS calculations used in the present study confirmed this observation.

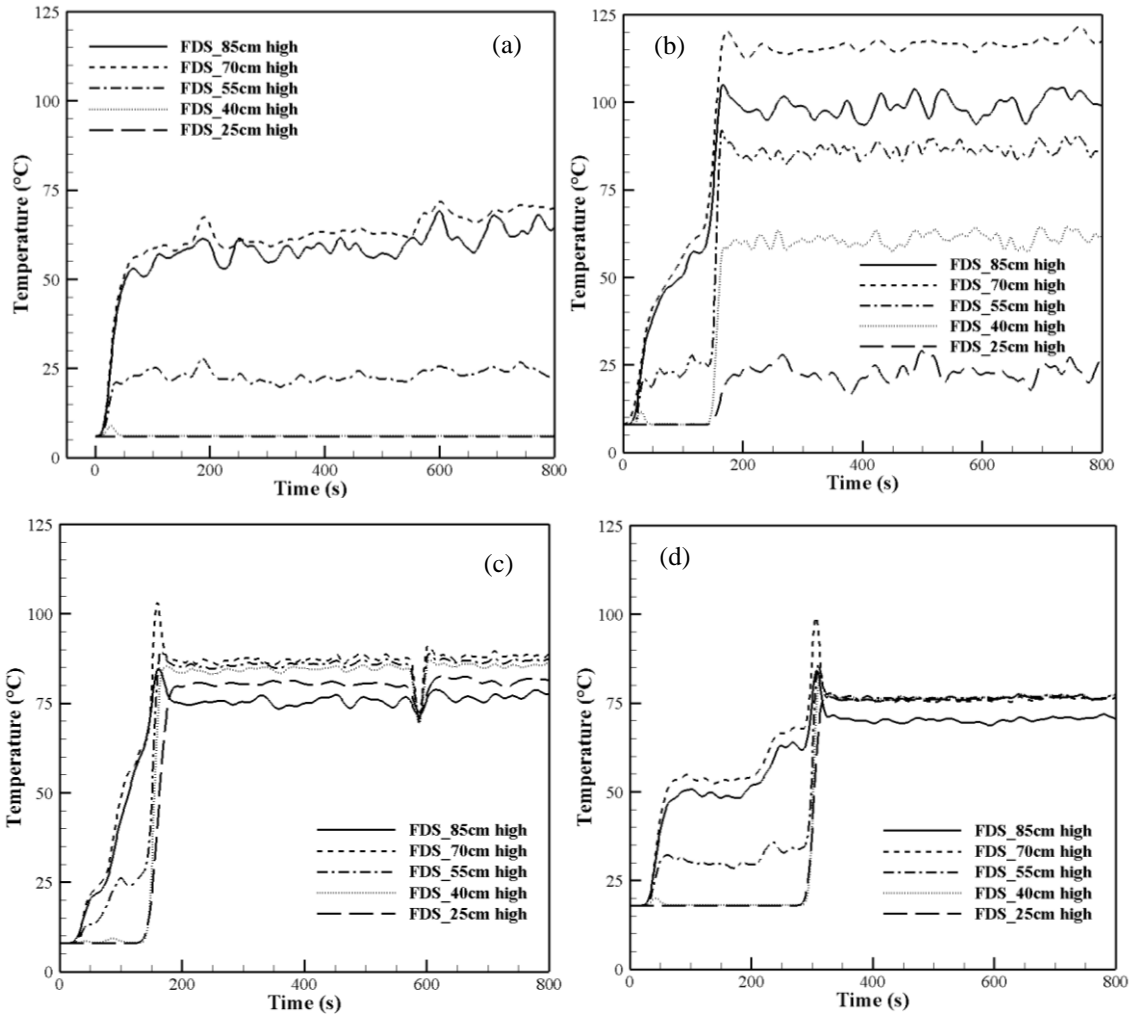


Fig. 5. Influence of wind velocity (a) $V_w=0$ m/s; (b) $V_w=1.73$ m/s; (c) $V_w=3.46$ m/s; (d) $V_w=5.20$ m/s on smoke temperature in different heights of the corridor

Fig. 5 presents the comparison between the smoke temperature near the ceiling and near the floor observed in the present study. It can be seen that the more wind speed increases, the more the smoke stratification is disturbed. Smoke stratification is represented by the stability between the hot zone and the cold zone. The hot zone is formed by hot smoke and the cold zone is formed by cold air. Smoke stratification in an enclosure is due to the temperature difference between these two zones. In addition, as shown by the studies reported in Ref. [39][40][41][42], smoke stratification depends on the Froude number (Fr). Smoke stratification is very stable up to a critical Fr and becomes disturbed when Fr is larger than this critical value. In this way, smoke stratification in an enclosure is related to the wind velocity that can also be generally expressed using Fr . In Fig. 5(a), when the wind velocity is 0 m/s, the smoke temperature near the ceiling and floor are about 5 °C and 60 °C, indicating that smoke stratification is very stable. At a wind velocity of 1.73 m/s i.e. $Fr=0.38$, the smoke temperature near the ceiling and floor are about 25 °C and 100 °C respectively. In this condition, there are still two zones. In Fig. 5(b), there is a slight perturbation of the temperature near the ceiling, indicating a slight disturbance in the smoke

stratification. However, from a wind velocity of 3.46 m/s i.e. $Fr=0.76$, the smoke temperature near the ceiling and floor are similar with an average of 80 °C. This means that above this velocity, there is no smoke stratification in the corridor and that smoke occupies the entire corridor. Under these conditions, there is a risk of toxicity for people. These observations confirm results reported in the literature [11] and highlight the ability of FDS to reproduce the effects of wind on the movement of smoke in an enclosure. Moreover, in these conditions, outdoor wind becomes a disturbance for smoke extraction, creating an unacceptable situation for fire safety.

The smoke temperature field with (a) $V_w=0$ m/s; (b) $V_w=1.73$ m/s; (c) $V_w=3.46$ m/s; (d) $V_w=5.20$ m/s in the cross section $y=0.5$ m at 300 s is shown in Fig. 6. It can be clearly seen that when there is no outdoor wind, there is temperature stratification in the corridor. In addition, the temperature near the ceiling is much higher than the temperature near the floor. For a wind velocity of 1.73 m/s i.e. $Fr=0.38$, smoke stratification is disturbed but still exists due to the presence of two zones, with a much smaller cold zone than hot zone. When the wind velocity is 3.46 m/s i.e. $Fr=0.76$, smoke stratification disappears, as the smoke temperature is similar at the different heights and only the hot zone subsists. In this condition, smoke occupies the entire corridor. The phenomenon of temperature stratification in the corridor disappears completely when the wind velocity reaches 5.20 m/s i.e. $Fr=1.1$ (Fig. 6(d)), as also shown with the curves in Fig. 5(d). These results also show that thanks to simulations performed by FDS, it is possible to demonstrate the fields of smoke movement in an enclosure with outdoor wind.

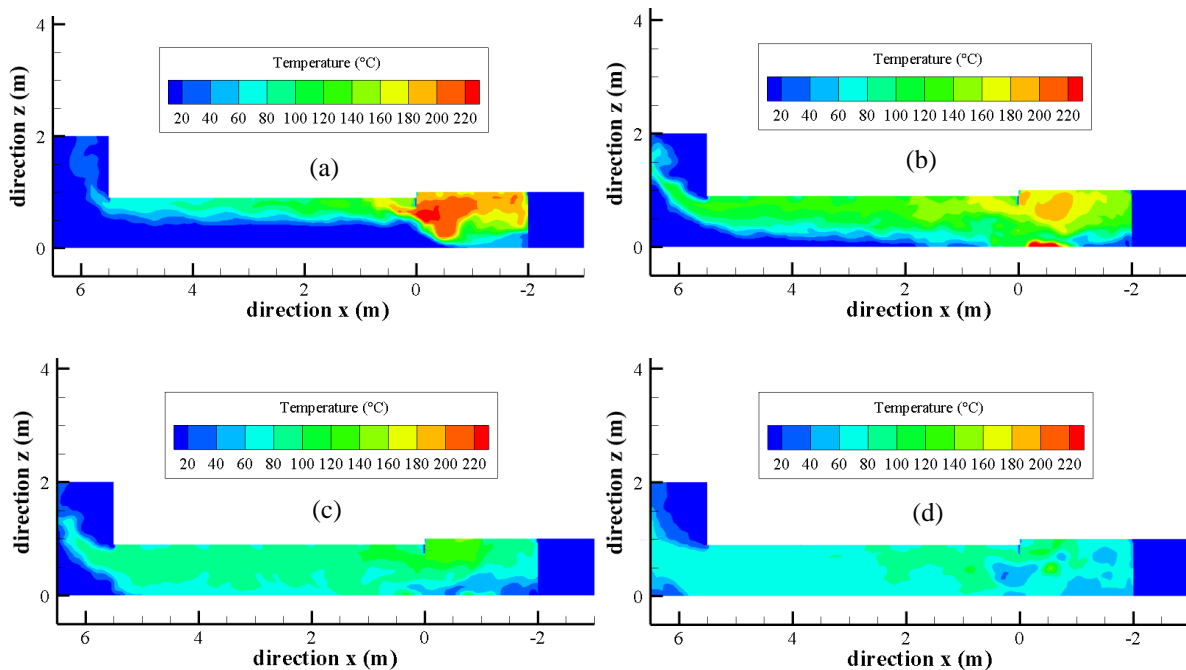


Fig. 6. Smoke temperature field with (a) $V_w=0$ m/s; (b) $V_w=1.73$ m/s; (c) $V_w=3.46$ m/s; (d) $V_w=5.20$ m/s on the cross section $y=0.5$ m at 300 s

It is concluded that smoke stratification state in the corridor depends on Fr and it can be divided into three cases:

When $Fr < 0.38$, smoke stratification in the corridor is stable. There is clear boundary between two zones: the upper hot zone and the lower cold zone in the corridor.

When $0.38 \leq Fr < 0.76$, smoke stratification in the corridor is unstable. Smoke stratification is slightly disturbed but still exists due to the presence of two zones, with a much smaller cold zone than hot zone.

When $Fr \geq 0.76$, smoke stratification in the corridor is completely disturbed with the similarity in smoke temperature at the different heights and only the hot zone exists. In this condition, smoke occupies the entire volume of the compartment, highlighting a risk of toxicity to people.

4.2. Effects of outdoor wind on smoke exhaust

Fig. 7 presents the smoke velocity field with (a) $V_w=0$ m/s; (b) $V_w=1.73$ m/s; (c) $V_w=3.46$ m/s; (d) $V_w=5.20$ m/s; (e) $V_w=6.93$ m/s; (f) $V_w=8.66$ m/s in the cross section $y=0.5$ m at 300 s. The cross section $y=0.5$ m is the plane in the middle of the corridor. In Fig. 7(a), taking this plane at the height of 70 cm, the maximum value of the smoke velocity is near the door and decreases with the distance from the door as shown in Fig. 3(b). In addition, taking into account smoke stratification with a hot zone near the ceiling and a cold zone near the floor, it is observed that the buoyancy effects give the reverse observation. Near the floor, the smoke velocity increases with the distance, and using the vortex recirculation solved by the Deardorff turbulence model, the numerical solver is able to reproduce the vortex flow induced by the smoke flow.

From Fig. 7, it can be seen that the maximum of smoke velocity in the corridor increases when the wind velocity increases. As mentioned previously, in these conditions smoke exhaust can be disturbed. Outdoor wind can however contribute to the evacuation of smoke and fire extinction in that more smoke is extracted through the corridor when the wind velocity increases. It should nevertheless be mentioned that while ventilation and extraction systems play an important role in fire engineering [17], the efficiency of the smoke extraction system will be reduced and even be invalidated when the outdoor wind velocity is very high and the extraction system is installed in the windward surface of the compartment [43]. In this case, the extraction system cannot perform well and smoke can spread along the entire compartment through the connected rooms. This situation is not acceptable for fire safety.

Fig. 8 and Fig. 9 show that when the outdoor wind velocity increases, the oxygen concentration increases and carbon dioxide concentration decreases. Fig. 8 presents the influence of wind velocity on O_2 concentration and CO_2 concentration at a height of 85 cm (on the ceiling of the corridor), showing that the more wind velocity increases, the more oxygen concentration increases. After 300 s, the oxygen concentration remains stable when

the wind velocity varies from 0 to 6.93 m/s. The oxygen concentration at 300 s was therefore used to compare the different wind velocity cases.

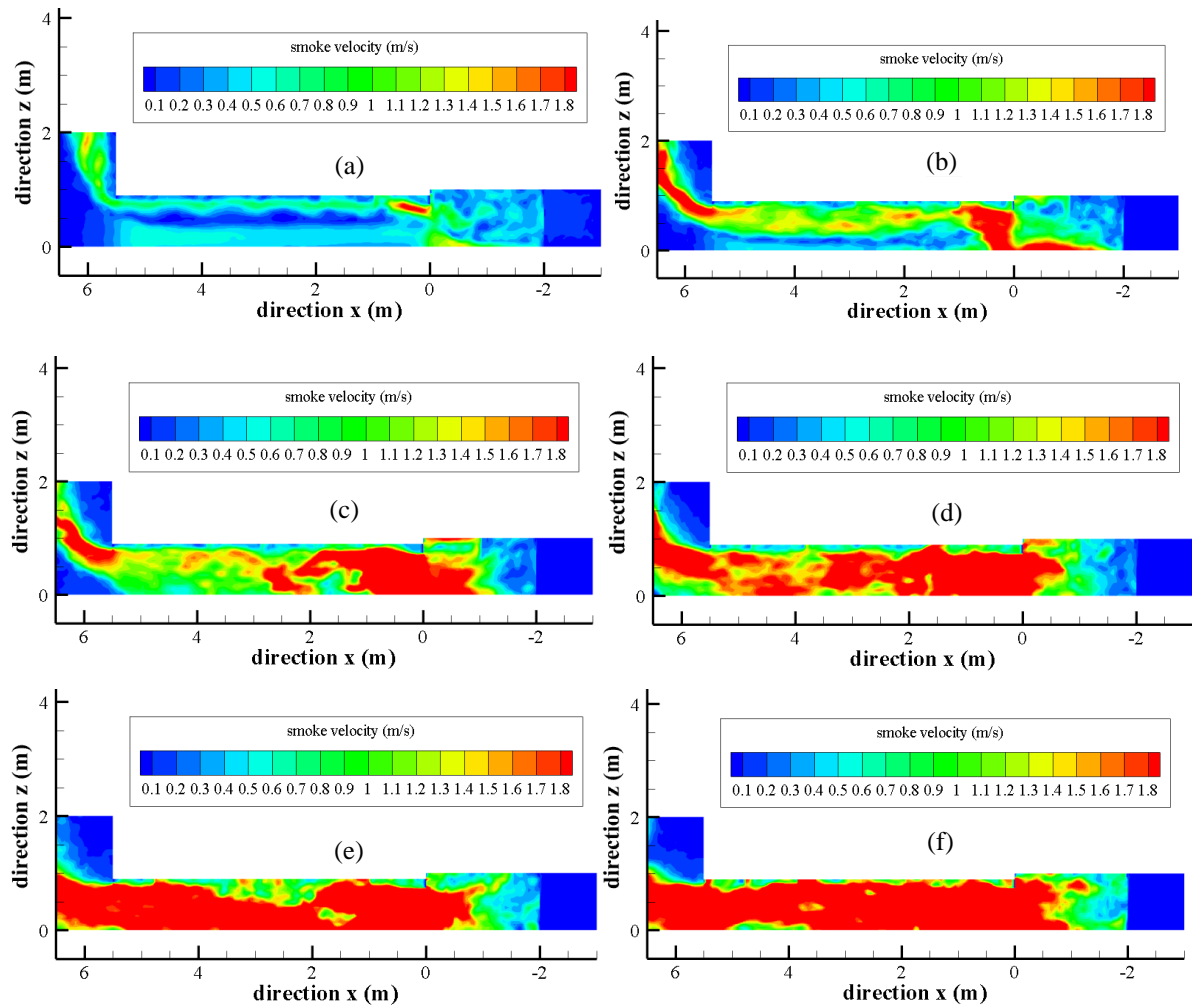


Fig. 7. Simulation of the smoke velocity field with (a) $V_w=0$ m/s; (b) $V_w=1.73$ m/s; (c) $V_w=3.46$ m/s; (d) $V_w=5.20$ m/s; (e) $V_w=6.93$ m/s; (f) $V_w=8.66$ m/s in the cross section $y=0.5$ m at 300 s

When the wind velocity is 1.73 m/s, the O_2 molar concentration increases only slightly compared to a situation without wind. When the wind velocity increases to 3.46 m/s, the O_2 molar concentration increases strongly compared to the case without wind. For a wind velocity of 6.93 m/s, the O_2 molar concentration increases to 20.2%, 1.8% higher than without wind. The rise in O_2 concentration in the corridor also indicates that more smoke is extracted.

The more the wind velocity increases, the more the CO_2 concentration decreases (Fig. 8(b)). At a wind velocity of 6.93 m/s, the CO_2 molar concentration decreases to 0.3%, 1% lower than without wind. The decline of the CO_2 concentration in the corridor also contributes to people escaping from fires.

Fig. 9 presents the oxygen concentration field with (a) $V_w=0$ m/s; (b) $V_w=1.73$ m/s; (c) $V_w=3.46$ m/s; (d) $V_w=5.20$ m/s in the cross section $y=0.5$ m at 300 s. It can be seen that the mean oxygen concentration in the corridor increases when wind velocity increases, showing that a higher wind velocity can facilitate smoke exhaust.

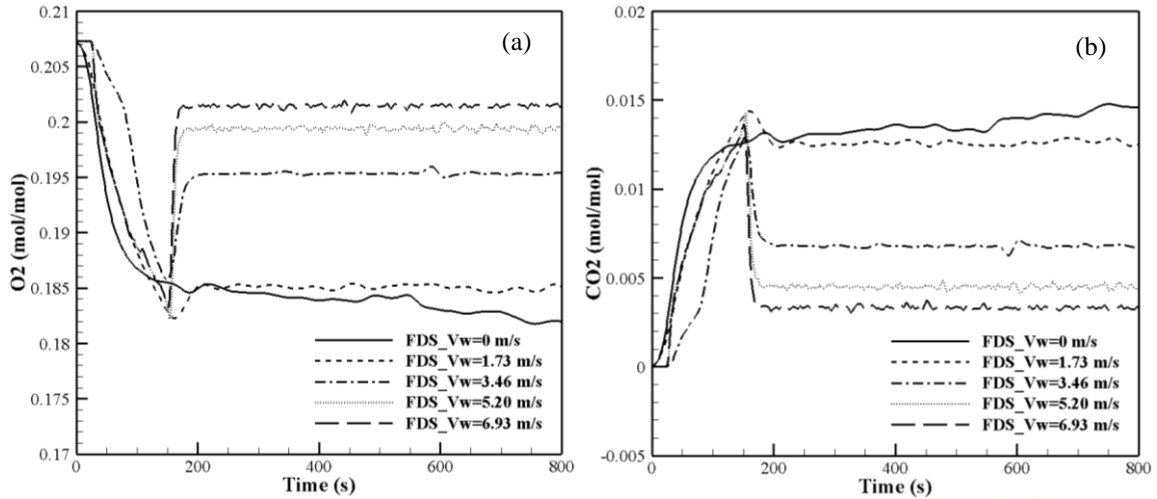


Fig. 8. Influence of wind velocity on: (a) O₂ concentration; (b) CO₂ concentration at 85 cm height

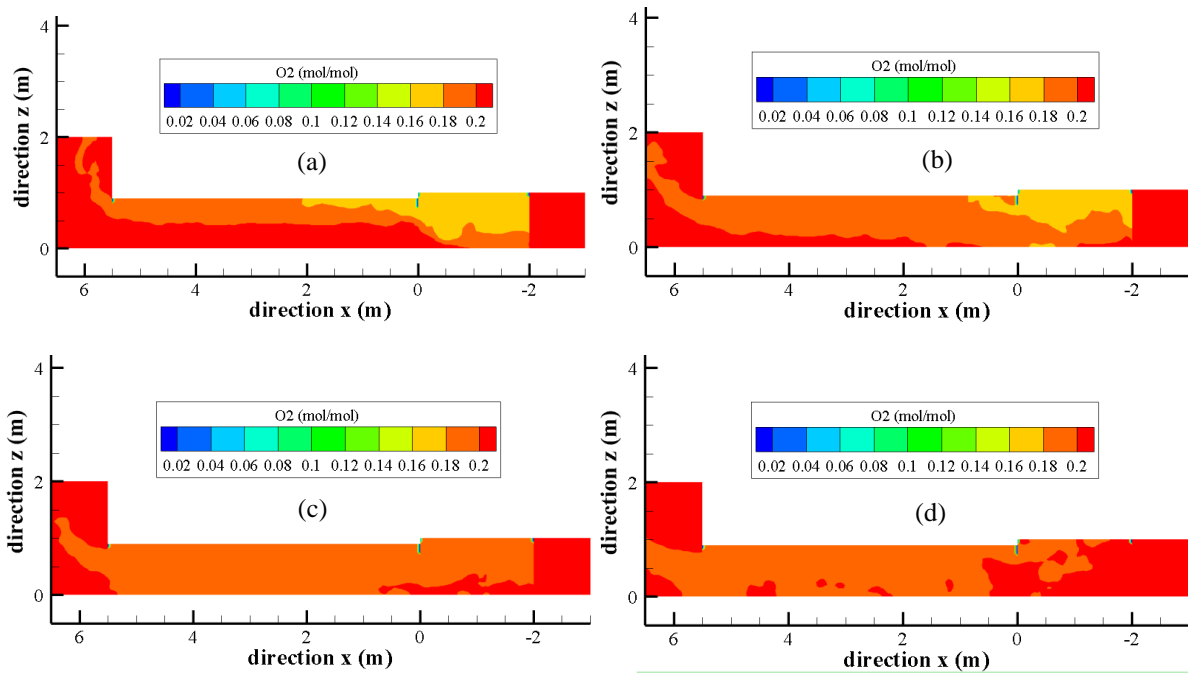


Fig. 9. Oxygen concentration field with (a) $V_w=0$ m/s; (b) $V_w=1.73$ m/s; (c) $V_w=3.46$ m/s; (d) $V_w=5.20$ m/s in the cross section $y=0.5$ m at 300 s

The influence of wind velocity on CO concentration and visibility at a height of 50 cm is plotted in Fig. 10. The height of 50 cm represents the average height of a person measuring 165 cm in a full-scale building. From Fig. 10(a), it can be seen that CO concentration decreases with wind velocity. The outdoor wind can thus be an advantage for diluting the CO concentration. Fig. 10(b) shows that the more the outdoor wind velocity increases, the more the visibility increases. Thus, the more wind blows in, the more smoke is diluted. However, the visibility becomes homogenous in the enclosure due to disturbance in the smoke stratification. In a fire with a heat release

rate larger than the one used in this study, the poor visibility can be unfavorable for the evacuation of people in the building.

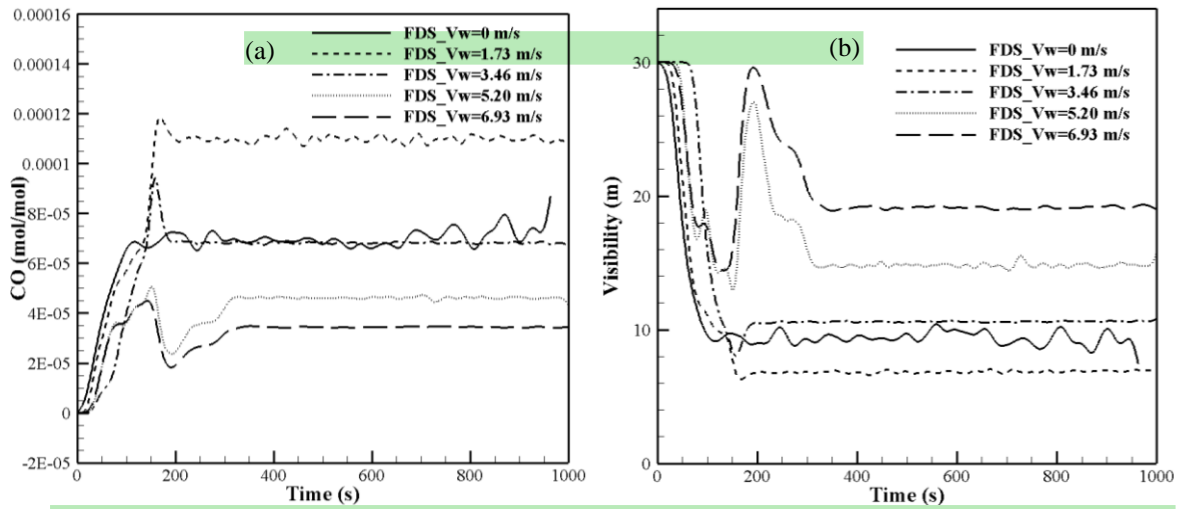


Fig. 10. Influence of wind velocity on: (a) CO concentration; (b) visibility at 55 cm height at the exit of the corridor

Fig. 11 presents the CO concentration field with (a) $V_w=0$ m/s; (b) $V_w=1.73$ m/s; (c) $V_w=3.46$ m/s; (d) $V_w=5.20$ m/s in the cross section $y=0.5$ m at 300 s. It can be seen that the average concentration of CO decreases with the increase in wind velocity. There are two zones: a thin zone near the floor and a thick zone near the ceiling in the case of no wind. The distribution of CO concentration in the corridor gradually becomes homogeneous as the wind velocity increases. Although in this study the CO concentration is so small that it would have little effect on people's health, the homogeneous distribution of CO concentration may cause serious problems when the heat release rate in the building is larger, producing more CO.

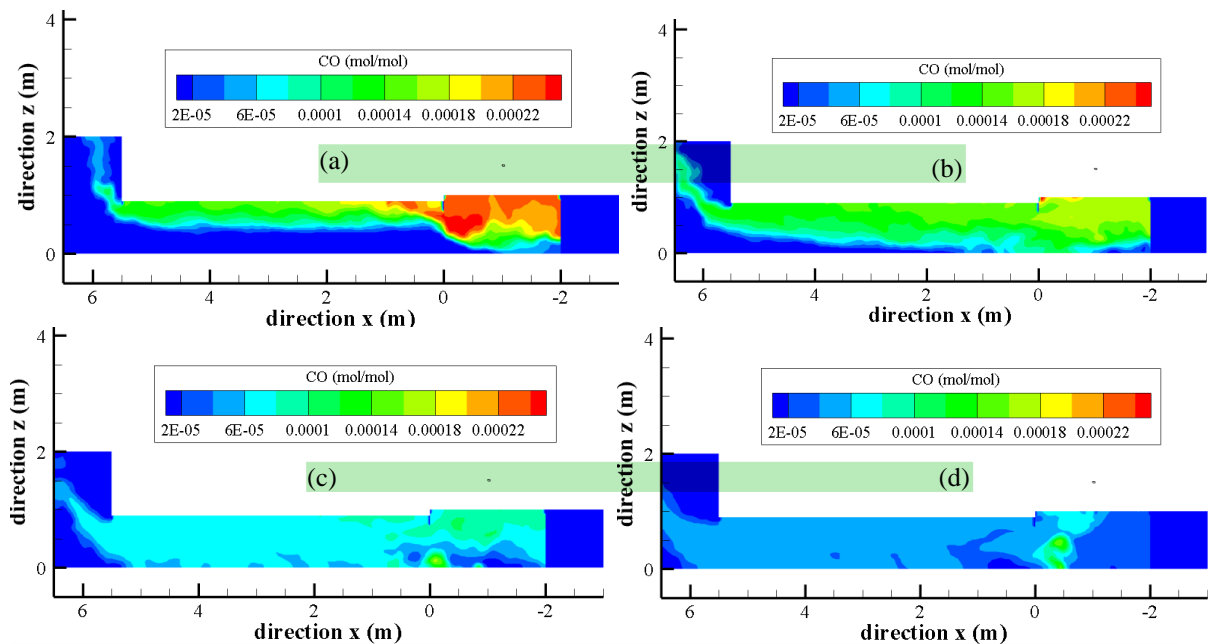


Fig. 11. CO concentration field with (a) $V_w=0$ m/s; (b) $V_w=1.73$ m/s; (c) $V_w=3.46$ m/s; (d) $V_w=5.20$ m/s in the cross section $y=0.5$ m at 300 s

Fig. 12 presents the visibility field with (a) $V_w=0$ m/s; (b) $V_w=1.73$ m/s; (c) $V_w=3.46$ m/s; (d) $V_w=5.20$ m/s in the cross section $y=0.5$ m at 300 s. Fig. 12(a) shows that the visibility of the lower area in the corridor is very high and the visibility of the upper area in the corridor is very low due to smoke stratification when there is no wind. The visibility in the corridor gradually becomes homogeneous as the outdoor wind velocity increases, and increases when the wind velocity reaches 5.20 m/s, indicating that the more smoke is exhausted, the more visibility is improved.

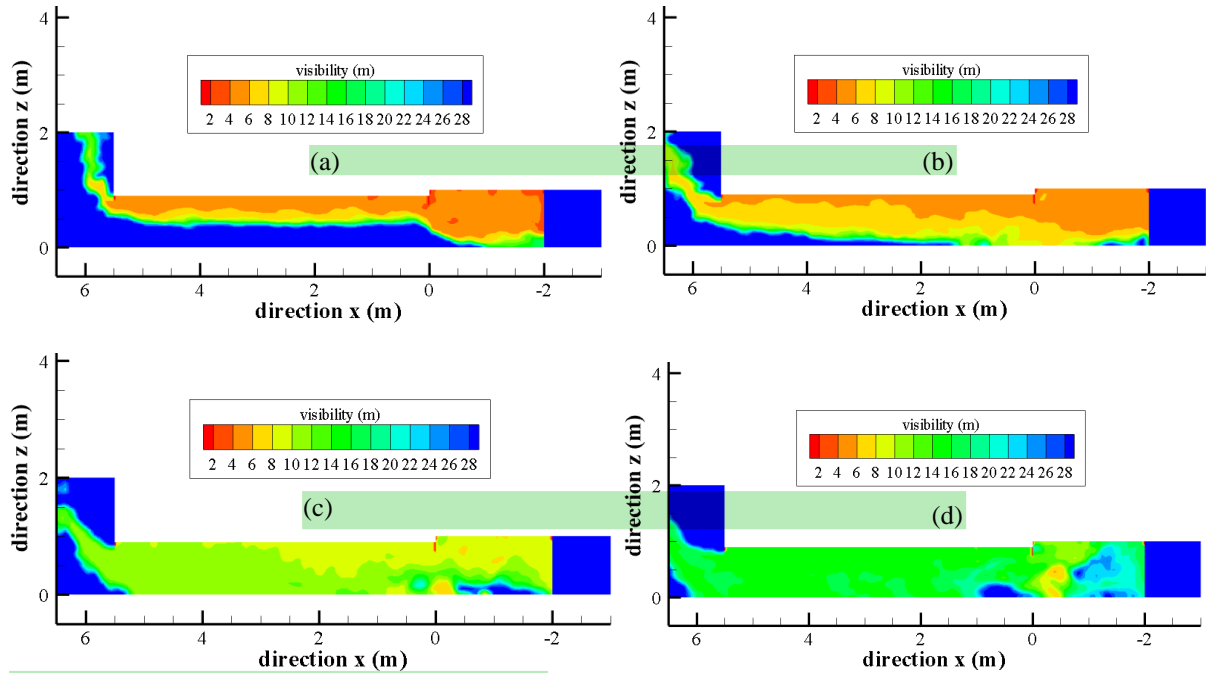


Fig. 12. Visibility field with (a) $V_w=0$ m/s; (b) $V_w=1.73$ m/s; (c) $V_w=3.46$ m/s; (d) $V_w=5.20$ m/s in the cross section $y=0.5$ m at 300 s

In other words, smoke can exit the corridor faster when the wind velocity increases. It can be said that to some extent, the outdoor wind is helpful for smoke exhaust and an advantage for the evacuation of people in fires as it can decrease the concentration of toxic gas and improve visibility in the environment. However, in these conditions, the outdoor wind becomes a disturbance for the extraction system, representing an unacceptable situation for fire safety.

4.3. Sensitivity analysis results

A global sensitivity analysis was carried out to investigate the relative importance of seven parameters: mass flux MF, activation energy E_a , conductivity λ , emissivity ϵ , pre-exponential factor A , density ρ and specific heat c_p . The aim was to determine whether, among these seven parameters, even a slight modification of the input parameter may cause a large variation in the response. The quantity of interest is the temperature near the ceiling.

A tolerance interval of $\pm 10\%$ was applied to each of the inputs so that for each of the inputs a dimensionless random parameter is introduced. Its value depends on the realization θ and belongs to the interval $[-1,1]$. For example, the values of the random parameters MF and E_a depend on their mean value \overline{MF} and $\overline{E_a}$, on the tolerance interval $\pm 10\%$, and on the random dimensionless parameter ξ_{MF} and ξ_{E_a} (whose values depend on the observation θ), such that:

$$\begin{aligned} MF(\theta) &= \overline{MF}(1 + 0.1 \xi_{MF}(\theta)) \\ E_a(\theta) &= \overline{E_a}(1 + 0.1 \xi_{E_a}(\theta)) \end{aligned} \quad (21)$$

Because of the evolution of the response over time, a time-averaged value of sensitivity indices can be computed as:

$$\overline{S}_i = \frac{1}{t_f} \int_0^{t_f} \tilde{S}_i(t) dt \quad \text{and} \quad \overline{St}_i = \frac{1}{t_f} \int_0^{t_f} \tilde{St}_i(t) dt \quad (22)$$

where t_f is the final time of the study.

Fig. 13 presents the results of a local sensitivity analysis, for which the local sensitivity of the output T is derived from its derivative with respect to the considered parameter. The methodology proposed by Chaos [33] was used.

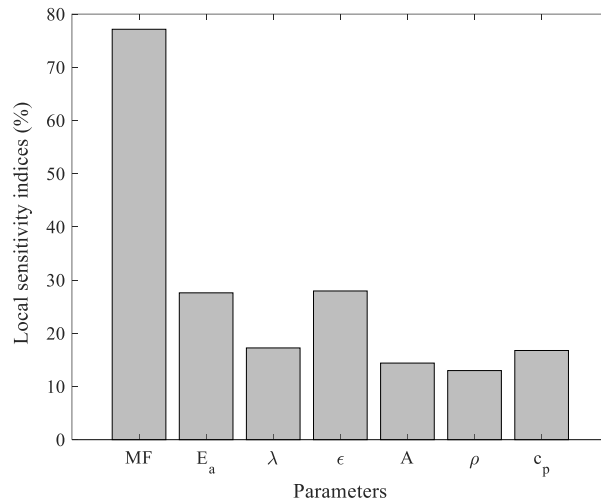


Fig. 13. Local sensitivity indices

Fig. 14 presents the first order sensitivity and the total sensitivity indices obtained by global sensitivity indices using PC expansion as presented in Section 3.

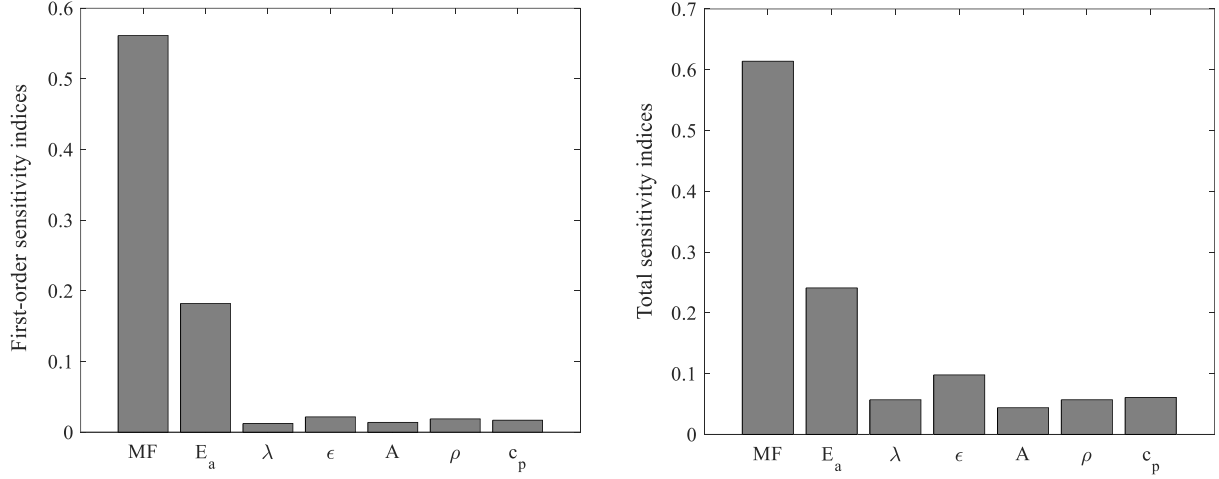


Fig. 14. First order (left) and total (right) Sobol' sensitivity indices

It can be observed that with the two methods, local and global with PC expansion, the mass flux is the most influential parameter. The second most influential parameter in both methods is the activation energy. However, the local method leads to a large sensitivity to variations in the emissivity, while it is nearly negligible in global sensitivity. The global sensitivity is a priori finer, because the range of variation of parameters is not very narrow (10%), and the number of samples taken to derive the sensitivity indices much greater (72 samples for global analysis, 8 samples for local analysis). Global sensitivity analysis was therefore chosen in this study.

These results show that the numerical results may vary significantly if the mass flux and the activation energy are not well quantified. To reduce this variance, one should work on reducing the tolerance interval of these two parameters in a first step.

Furthermore, sensitivity analysis makes it possible to reduce the model physically. Even though a quantitative difference is observed between first-order and total sensitivity indices, meaning that coupling effects between several parameters occur, the model can be simplified by taking only the mass flux and the activation energy as inputs. This reduction is also justified by observing the bar plot of the time-averaged absolute value of the stochastic coefficients presented in Fig. 15. This quantity is defined for each stochastic mode i by:

$$\bar{Y}_{\alpha_i} = \frac{1}{t_f} \int_0^{t_f} |Y_{\alpha_i}(t)| dt \quad (23)$$

Among the stochastic modes, it was shown earlier that the first coefficient ($\alpha_1 = \{0,0,0,0,0,0,0\}$) represents directly the mean of the random process. Hence, its value is much larger than the values of the other stochastic modes. Thus, in Fig. 15 the 36 stochastic coefficients \bar{Y}_{α_i} except for the first one are plotted.

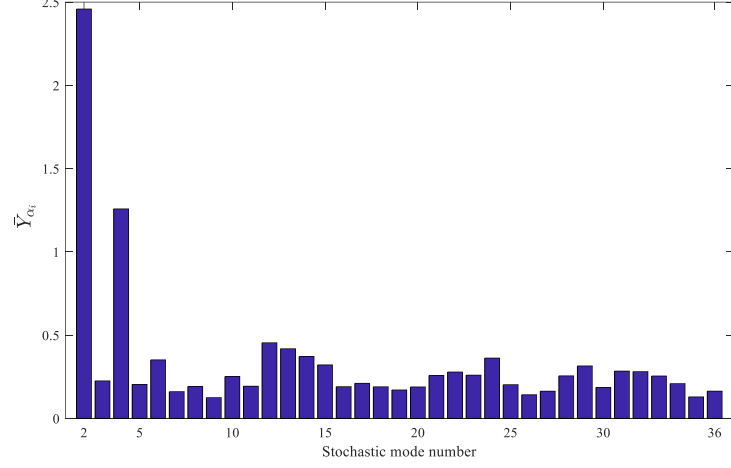


Fig. 15. Time-averaged absolute values of the stochastic coefficients

Fig. 15 shows that among all modes, two have a larger time-averaged value: the second mode corresponding to the set $\alpha_2 = \{1,0,0,0,0,0\}$ and the fourth mode corresponding to $\alpha_4 = \{0,1,0,0,0,0\}$. This implies that the quantity of interest T can be written as a linear function of the mass flux and of the activation energy:

$$T(t, MF, E_a, \lambda, \epsilon, A, \rho, C_p) \approx \tilde{T}(t, MF, E_a) \quad (24)$$

where $\tilde{T}(t, MF, E_a) = Y_{\alpha_1}(t) + \sqrt{3}Y_{\alpha_2}(t)\xi_{MF} + \sqrt{3}Y_{\alpha_4}(t)\xi_{E_a}$

A least square curve fitting can be applied on the stochastic coefficients $Y_{\alpha_1}(t)$, $Y_{\alpha_2}(t)$ and $Y_{\alpha_4}(t)$ resulting in the following approximations:

$$Y_{\alpha_1}(t) \approx \hat{Y}_{\alpha_1}(t) = \begin{cases} T_0, & t < 27s \\ T_0 + A \left(1 - \exp\left(-\frac{t}{\tau}\right)\right) + Bt + C, & t \geq 27s \end{cases} \quad (25)$$

$$Y_{\alpha_2}(t) \approx \hat{Y}_{\alpha_2} = 2.46 \text{ (}^\circ\text{C)} \quad (26)$$

$$Y_{\alpha_4}(t) \approx \hat{Y}_{\alpha_4}(t) = 1.5 \cdot 10^{-3} t - 2.1 \text{ (}^\circ\text{C)} \quad (27)$$

with $T_0=6 \text{ }^\circ\text{C}$, $A=32 \text{ }^\circ\text{C}$, $\tau=25s$, $B=16.5 \cdot 10^{-3} \text{ }^\circ\text{C /s}$ and $C=13.3 \text{ }^\circ\text{C}$. Such a decomposition can be very useful as the characteristic time τ provides information on the rate of increase of the temperature at the beginning of the fire, while the other parameters provide information on the evolution of the temperature amplitude and on the slope of the increase in temperature for large times. Fig. 16 and Fig. 17 show good agreement between the computed stochastic modes and their analytical approximations. Using these approximated coefficients, a reduced analytical metamodel \hat{T} is defined:

$$\hat{T}(t, MF, E_a) = \hat{Y}_{\alpha_1}(t) + \sqrt{3}\hat{Y}_{\alpha_2}\xi_{MF} + \sqrt{3}\hat{Y}_{\alpha_4}(t)\xi_{EA} \quad (28)$$

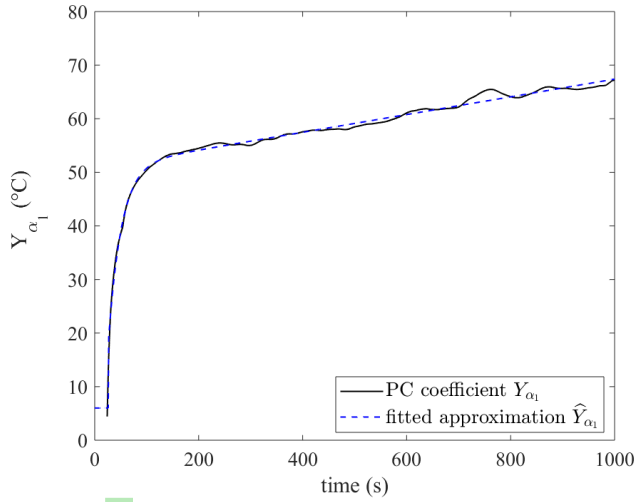


Fig. 16. Comparison between the mean response of the metamodel: Y_{α_1} and the fitted function \hat{Y}_{α_1}

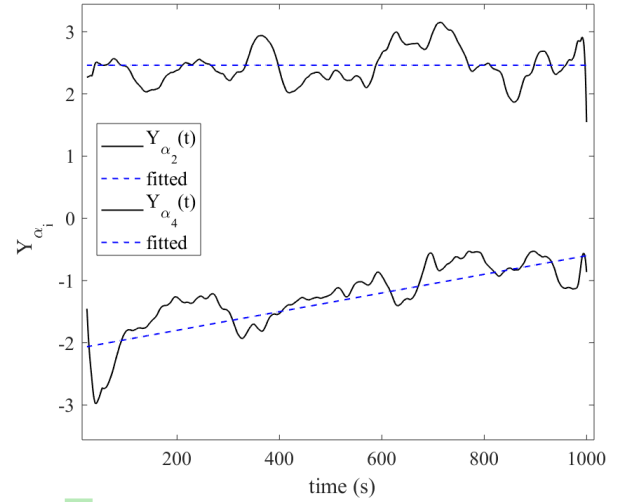


Fig. 17. Comparison between the stochastic coefficients Y_{α_2} and Y_{α_4} , and their fitted approximations \hat{Y}_{α_2} and \hat{Y}_{α_4}

Finally, the mean response and variance obtained with the empirical design and the metamodel \hat{T} using a reduced number of coefficients and interpolation are compared in Fig. 18 and Fig. 19. A close agreement can be observed in Fig. 18 for the mean response of the temperature for random input parameters. PC approximation leads to a good approximation of the model as the empirical variance is correctly represented when no mode truncation is applied. With mode truncation and the metamodel \hat{T} however, the variance of the quantity of interest for random input parameters is underestimated. Finally, Fig. 20 presents a comparison between the 72 samples obtained for different values of input parameters, and the mean and the envelope obtained by the analytical metamodel \hat{T} , using a $[-3\hat{\sigma}, 3\hat{\sigma}]$ confidence interval, $\hat{\sigma}$ being the standard deviation of the metamodel \hat{T} , defined by:

$$\hat{\sigma}^2 = \text{var}\left(\hat{T}(t, MF, E_a)\right) = \hat{Y}_{\alpha_2}^2 + \hat{Y}_{\alpha_4}(t)^2 \quad (29)$$

It can be seen that using this confidence interval provides a very close prediction of the temperature on the entire time range, even if the simplified metamodel has only 2 input parameters, while for the 72 simulated samples, each of the seven input parameters was random.

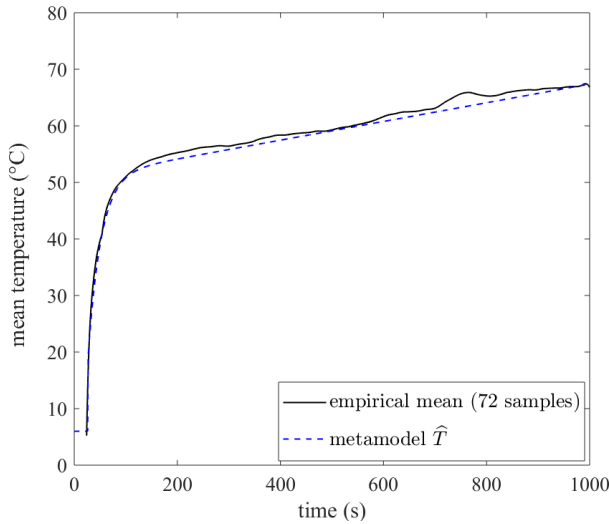


Fig. 18. Comparison of the mean response of the experimental design and the proposed fitting function \hat{T}

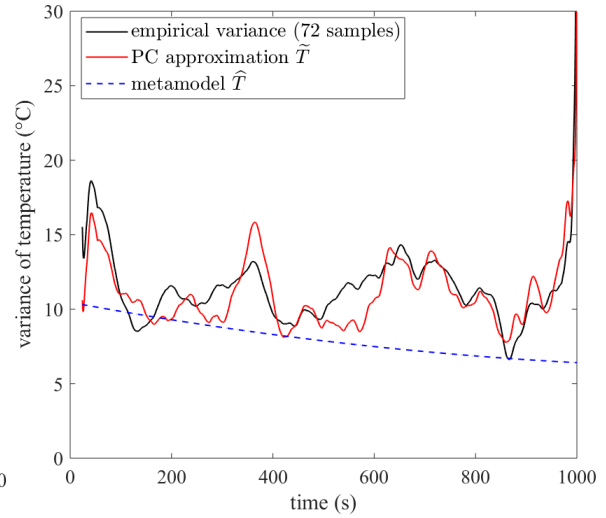


Fig. 19. Comparison between variance of the experimental design and the proposed fitting function

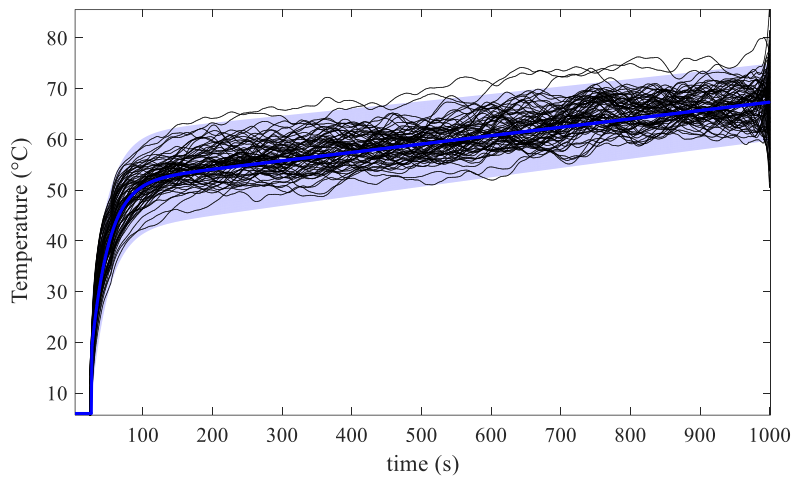


Fig. 20. Comparison between the 72 samples (black thin lines) and the analytical metamodel in blue (mean response in thick line, $[-3\hat{\sigma}, 3\hat{\sigma}]$ confidence interval in filled area) (colors online)

5. Conclusion

In this study, a CFD code, namely FDS (Fire Dynamics Simulator), was employed to model the smoke spreading along a corridor induced by a compartment fire. The main focus was on the effects of outdoor wind on the dynamics of smoke spreading based on experimental data. Simulations were carried out by varying wind velocity from 0 to 12.12 m/s. Good agreement between experimental data and prediction was found, enabling investigation of smoke stratification, smoke exhaust and a global sensitivity analysis. The major findings include: (1) By analyzing the temperature distribution in the corridor, it was found that smoke stratification in the corridor can be strongly affected by the outdoor wind. For that, three thermal buoyant flow stratifications were found: stable buoyant stratification ($Fr < 0.38$), unstable buoyant stratification ($0.38 \leq Fr < 0.76$) and failed stratification

($Fr \geq 0.76$). When $Fr \geq 0.76$, smoke stratification in the corridor is completely disturbed and smoke occupies the entire volume of the compartment, highlighting a risk of toxicity to people.

(2) When the wind velocity is higher than the critical value (here 3.46 m/s), O_2 concentration and visibility increase while CO_2 and CO concentration tend to decrease. It is shown that the magnitude of the outdoor wind can facilitate smoke exhaust in a compartment fire.

(3) The results of a global sensitivity analysis indicate that it is essential to define the most influential input parameters correctly, namely the mass flux of the fuel and the activation energy. If not, large deviations in the outputs of the numerical results such as smoke temperature may occur due to variations, even slight ones, in the input parameters.

(4) Based on the amplitude of the metamodel coefficients, a reduced metamodel has been proposed. A prediction with a confidence interval can be easily implemented, leading to close agreement with the numerical results.

Through this work, it is demonstrated that CFD FDS is capable of providing information with regard to the movement of smoke in a corridor. Besides, it can be coupled with a Polynomial Chaos-based sensitivity analysis, which enables the input parameters to be classified on quantitative grounds with a limited computational cost.

Acknowledgement

The authors thank the reviewers for their valuable comments on the initial version of this paper.

References

- [1] Y.-T. E, L. Zhou, The Research on the Current Safety Status of High-rise Building at Home and Abroad, *Procedia Eng.* 135 (2016) 574–577. doi:10.1016/j.proeng.2016.01.108.
- [2] K.T. Paul, T.R. Hull, K. Lebek, A.A. Stec, Fire smoke toxicity: The effect of nitrogen oxides, *Fire Saf. J.* 43 (2008) 243–251. doi:10.1016/j.firesaf.2007.10.003.
- [3] T.R. Hull, D. Brein, A.A. Stec, Quantification of toxic hazard from fires in buildings, *J. Build. Eng.* 8 (2016) 313–318. doi:10.1016/j.jobe.2016.02.014.
- [4] L. Hu, F. Ren, K. Hu, F. Tang, K. Lu, An experimental study on temperature evolution inside compartment with fire growth and flame ejection through an opening under external wind, *Proc. Combust. Inst.* 36 (2017) 2955–2962. doi:10.1016/j.proci.2016.06.069.
- [5] X. Sun, X. Zhang, L. Hu, K. Kuwana, Temperature evolution and transition inside fire compartment with an opening subject to external sideward wind, *Proc. Combust. Inst.* 000 (2018) 1–9. doi:10.1016/j.proci.2018.05.161.
- [6] L. Hu, K. Hu, F. Ren, X. Sun, Facade flame height ejected from an opening of fire compartment under external

- wind, *Fire Saf. J.* 92 (2017) 151–158. doi:10.1016/j.firesaf.2017.06.008.
- [7] M. Li, Z. Gao, J. Ji, K. Li, J. Sun, Wind effects on flame projection probability from a compartment with opposing openings, *Fire Saf. J.* 91 (2017) 414–421. doi:10.1016/j.firesaf.2017.04.037.
- [8] C. Fan, L. Zhang, S. Jiao, Z. Yang, M. Li, X. Liu, Smoke spread characteristics inside a tunnel with natural ventilation under a strong environmental wind, *Tunn. Undergr. Sp. Technol.* 82 (2018) 99–110. doi:10.1016/j.tust.2018.08.004.
- [9] X. Tian, M. Zhong, C. Shi, P. Zhang, C. Liu, Full-scale tunnel fire experimental study of fire-induced smoke temperature profiles with methanol-gasoline blends, *Appl. Therm. Eng.* 116 (2017) 233–243. doi:10.1016/j.applthermaleng.2017.01.099.
- [10] M.H. Zhong, C.L. Shi, L. He, J.H. Shi, C. Liu, X.L. Tian, Smoke development in full-scale sloped long and large curved tunnel fires under natural ventilation, *Appl. Therm. Eng.* 108 (2016) 857–865. doi:10.1016/j.applthermaleng.2016.07.141.
- [11] S.C. Li, D.F. Huang, N. Meng, L.F. Chen, L.H. Hu, Smoke spread velocity along a corridor induced by an adjacent compartment fire with outdoor wind, *Appl. Therm. Eng.* 111 (2017) 420–430. doi:10.1016/j.applthermaleng.2016.09.086.
- [12] F. Tang, Q. He, F. Mei, Q. Shi, L. Chen, K. Lu, Fire-induced temperature distribution beneath ceiling and air entrainment coefficient characteristics in a tunnel with point extraction system, *Int. J. Therm. Sci.* 134 (2018) 363–369. doi:10.1016/j.ijthermalsci.2018.08.023.
- [13] F. Tang, Q. He, F. Mei, Q. Wang, H. Zhang, Effect of ceiling centralized mechanical smoke exhaust on the critical velocity that inhibits the reverse flow of thermal plume in a longitudinal ventilated tunnel, *Tunn. Undergr. Sp. Technol.* 82 (2018) 191–198. doi:10.1016/j.tust.2018.08.039.
- [14] C.G. Fan, J. Ji, Z.H. Gao, J.H. Sun, Experimental study on transverse smoke temperature distribution in road tunnel fires, *Tunn. Undergr. Sp. Technol.* 37 (2013) 89–95. doi:10.1016/j.tust.2013.04.005.
- [15] J.G. Quintiere, *Fundamentals of Fire Phenomena*, 2006. doi:10.1002/0470091150.ch12.
- [16] J. Lassus, L. Courty, J.P. Garo, E. Studer, P. Jourda, P. Aine, Ventilation effects in confined and mechanically ventilated fires, *Int. J. Therm. Sci.* 75 (2014) 87–94. doi:10.1016/j.ijthermalsci.2013.07.015.
- [17] A. Li, Y. Zhang, J. Hu, R. Gao, Reduced-scale experimental study of the temperature field and smoke development of the bus bar corridor fire in the underground hydraulic machinery plant, *Tunn. Undergr. Sp. Technol.* 41 (2014) 95–103. doi:10.1016/j.tust.2013.11.009.
- [18] W. Zhao, R. Zong, X. Fan, X. Zhao, Impact of openings on fire properties in the confined corridors, *Appl. Therm. Eng.* 110 (2017) 746–757. doi:10.1016/j.applthermaleng.2016.08.206.
- [19] G.S. Yang, Y.L. An, L.M. Peng, J.H. Zhang, Simulation of smoke flow and longitudinal ventilation in tunnel fire, *Trans. Nonferrous Met. Soc. China (English Ed.)* 16 (2006) 741–746. doi:10.1016/S1003-6326(06)60131-3.
- [20] O. Vauquelin, Experimental simulations of fire-induced smoke control in tunnels using an “air-helium reduced

- scale model": Principle, limitations, results and future, *Tunn. Undergr. Sp. Technol.* 23 (2008) 171–178.
doi:10.1016/j.tust.2007.04.003.
- [21] M.C. Weng, L.X. Yu, F. Liu, P. V. Nielsen, Full-scale experiment and CFD simulation on smoke movement and smoke control in a metro tunnel with one opening portal, *Tunn. Undergr. Sp. Technol.* 42 (2014) 96–104.
doi:10.1016/j.tust.2014.02.007.
- [22] B. Batiot, T. Rogaume, A. Collin, F. Richard, J. Luche, Sensitivity and uncertainty analysis of Arrhenius parameters in order to describe the kinetic of solid thermal degradation during fire phenomena, *Fire Saf. J.* 82 (2016) 76–90.
doi:10.1016/j.firesaf.2016.03.007.
- [23] S. Xiao, Z. Lu, P. Wang, Multivariate global sensitivity analysis for dynamic models based on wavelet analysis, *Reliab. Eng. Syst. Saf.* 170 (2018) 20–30. doi:10.1016/j.res.2017.10.007.
- [24] M. Lamboni, D. Makowski, S. Lehuger, B. Gabrielle, H. Monod, Multivariate global sensitivity analysis for dynamic crop models, *F. Crop. Res.* 113 (2009) 312–320. doi:10.1016/j.fcr.2009.06.007.
- [25] G. Blatman, B. Sudret, Efficient computation of global sensitivity indices using sparse polynomial chaos expansions, *Reliab. Eng. Syst. Saf.* 95 (2010) 1216–1229. doi:10.1016/j.res.2010.06.015.
- [26] K. McGrattan, R. McDermott, Sixth Edition Fire Dynamics Simulator User 's Guide, (2016).
doi:10.6028/NIST.SP.1019.
- [27] K. McGrattan, S. Hostikka, R. McDermott, J. Floyd, C. Weinschenk, K. Overholt, Fire Dynamics Simulator Technical Reference Guide Volume 1: Mathematical Model, NIST Spec. Publ. 1018-1. 1 (2017).
doi:10.6028/NIST.SP.1018.
- [28] W. Gropp, E. Lusk, A. Skjellum, Using MPI : portable parallel programming with the message-passing interface, MIT Press, 1999.
- [29] J.W. Deardorff, Stratocumulus-capped mixed layers derived from a three-dimensional model, *Boundary-Layer Meteorol.* 18 (1980) 495–527. doi:10.1007/BF00119502.
- [30] I. Sellami, B. Manescau, K. Chetehouna, C. de Izarra, R. Nait-Said, F. Zidani, BLEVE fireball modeling using Fire Dynamics Simulator (FDS) in an Algerian gas industry, *J. Loss Prev. Process Ind.* 54 (2018) 69–84.
doi:10.1016/j.jlp.2018.02.010.
- [31] B. Magnognou, J.P. Garo, B. Coudour, H.Y. Wang, Risk analysis of unburnt gas ignition in an exhaust system connected to a confined and mechanically ventilated enclosure fire, *Fire Saf. J.* 91 (2017) 291–302.
doi:10.1016/j.firesaf.2017.03.036.
- [32] D. Menage, K. Chetehouna, W. Mell, Numerical simulations of fire spread in a Pinus pinaster needles fuel bed, *J. Phys. Conf. Ser.* 395 (2012). doi:10.1088/1742-6596/395/1/012011.
- [33] M. Chaos, Application of sensitivity analyses to condensed-phase pyrolysis modeling, *Fire Saf. J.* 61 (2013) 254–264. doi:10.1016/j.firesaf.2013.09.016.
- [34] A. Saltelli, M. Ratto, S. Tarantola, F. Campolongo, Sensitivity analysis practice: A guide to scientific models, 2006.

doi:10.1016/j.res.2005.11.014.

- [35] I.M. Sobol, Sensitivity analysis for nonlinear mathematical models, *Math. Model. Comput.* 1 (1993) 407–414. doi:10.18287/0134-2452-2015-39-4-459-461.
- [36] T. Crestaux, O. Le Maître, J.M. Martinez, Polynomial chaos expansion for sensitivity analysis, *Reliab. Eng. Syst. Saf.* 94 (2009) 1161–1172. doi:10.1016/j.res.2008.10.008.
- [37] D. Xiu, D. Lucor, C.-H. Su, G.E. Karniadakis, Stochastic Modeling of Flow-Structure Interactions Using Generalized Polynomial Chaos, *J. Fluids Eng.* 124 (2002) 51. doi:10.1115/1.1436089.
- [38] M. Eldred, J. Burkardt, Comparison of Non-Intrusive Polynomial Chaos and Stochastic Collocation Methods for Uncertainty Quantification, in: 47th AIAA Aerosp. Sci. Meet. Incl. New Horizons Forum Aerosp. Expo., American Institute of Aeronautics and Astronautics, Reston, Virginia, 2009. doi:10.2514/6.2009-976.
- [39] J.S. Newman, Experimental Evaluation of Fire-Induced Stratification, *Combust. Flame.* 39 (1984) 33–39.
- [40] F. Tang, L.J. Li, M.S. Dong, Q. Wang, F.Z. Mei, L.H. Hu, Characterization of buoyant flow stratification behaviors by Richardson (Froude) number in a tunnel fire with complex combination of longitudinal ventilation and ceiling extraction, *Appl. Therm. Eng.* 110 (2017) 1021–1028. doi:10.1016/j.applthermaleng.2016.08.224.
- [41] D.F. Huang, S.C. Li, An experimental investigation of stratification characteristic of fire smoke in the corridor under the effect of outdoor wind, *J. Wind Eng. Ind. Aerodyn.* 179 (2018) 173–183. doi:10.1016/j.jweia.2018.05.021.
- [42] D. Yang, L.H. Hu, R. Huo, Y.Q. Jiang, S. Liu, F. Tang, Experimental study on buoyant flow stratification induced by a fire in a horizontal channel, *Appl. Therm. Eng.* 30 (2010) 872–878. doi:10.1016/j.applthermaleng.2009.12.019.
- [43] L. Yi, Y. Gao, J.L. Niu, S.J. Yang, Study on effect of wind on natural smoke exhaust of enclosure fire with a two-layer zone model, *J. Wind Eng. Ind. Aerodyn.* 119 (2013) 28–38. doi:10.1016/j.jweia.2013.05.005.